Journal of Volcanology and Geothermal Research 352 (2018) 106–116

Contents lists available at ScienceDirect

Journal of Volcanology and Geothermal Research

journal homepage: www.elsevier.com/locate/jvolgeores

Deformation patterns, magma supply, and magma storage at Karymsky Volcanic Center, Kamchatka, Russia, 2000–2010, revealed by InSAR

Lingyun Ji [a], Pavel Izbekov [b], Sergey Senyukov [c], Zhong Lu [d,*]

[a] The Second Monitoring and Application Center, China Earthquake Administration, Xi'an, Shaanxi, China
[b] Geophysical Institute, University of Alaska Fairbanks, Fairbanks, AK, USA
[c] Kamchatkan Branch of Geophysical Survey, Petropavlovsk-Kamchatsky, Russia
[d] Roy M. Huffington Department of Earth Sciences, Southern Methodist University, Dallas, TX, USA

ARTICLE INFO

Article history:
Received 28 August 2017
Received in revised form 23 December 2017
Accepted 15 January 2018
Available online 31 January 2018

ABSTRACT

Under a complex geological region influenced by the subduction of the Pacific plate, Kamchatka Peninsula is one of the most active volcanic arcs in the Pacific Rim. Due to logistical difficulty in instrumentation, shallow magma plumbing systems beneath some of the Kamchatkan volcanoes are poorly understood. InSAR offers a safe and quick method for monitoring volcanic deformation with a high spatial resolution. In this study, a group of satellite radar interferograms that span the time interval from 2000 to 2010 shows eruptive and non-eruptive deformation at Karymsky Volcanic Center (KVC), Kamchatka, Russia. All the interferograms provide details of the activity around the KVC during 2000–2010, as follows: (1) from 2000 to 2004, the Karymsky-AN (Akademia Nauk) area deflated and the MS (Maly Semyachik) area inflated, (2) from 2004 to 2006, the Karymsky-AN area deflated with ongoing eruption, while the MS area subsided without eruption, (3) from 2006 to 2008, as with 2000–2004, the Karymsky-AN area deflated and the MS area inflated, (4) from 2008 to 2010, the Karymsky-AN area inflated up to 3 cm, and the MS area subsided. Point source models suggest that two magma reservoirs provide a good fit to the observed deformation. One source is located beneath the area between Karymsky and AN at a depth of approximately 7.0 km, and the other one is situated beneath MS at a depth of around 5.8 km. Synchronous deformation patterns suggest that two magma systems are fed from the same deep magma source and connected by a fracture zone. The InSAR results are consistent with GPS ground deformation measurements, seismic data, and petrological constraints.

1. Introduction

Karymsky Volcanic Center (KVC), situated in the middle of the Eastern Volcanic Front (EVF) of Kamchatka, Russia, consists of a group of volcanoes, calderas and maars, with activity starting at about 3 Ma ago (e.g. Bindeman et al., 2010 and references therein; Masurenkov, 1980). Three of the KVC volcanoes, — Karymsky, Akademia Nauk (hereafter referred to as AN), and Maly Semyachik (hereafter referred to as MS) – erupted in the 20th century (Fig. 1).

Karymsky volcano is a stratovolcano situated in the middle of a 5-km-diameter caldera formed about 7900 years. BP (Braitseva and Melekestsev, 1991). The stratovolcano restarted to grow about 5300 BP through intermittent effusive and explosive activity, which ended about 2600 BP. The volcano resumed its eruptive activity approximately 500 years ago, with an intensity that has remained nearly constant until present. Numerous times during the 20th century, Karymsky has been in a state of continuous eruptive activity including 1908–1915, 1921–1925, 1929–1935, 1943–1947, 1952–1967, and 1970–1982 (Fischer et al., 2002 and references therein). The most recent cycle of activity began in January 1996 and ceased in October 2016 (Muravyev et al., 1998; Eichelberger and Izbekov, 2000; Izbekov et al., 2002; Rowell et al., 2014; Global Volcanism Program, 2016; Flower and Kahn, 2017). The eruptive behavior is usually described as Vulcanian, being confined to a short, regular explosions often accompanied by eruptions of blocky lava flows and gas-ash (Firstov et al., 2013; Lopez et al., 2014).

The AN caldera is centered about 9 km south of Karymsky (Fig. 1). It was formed 28,000–48,000 years ago (Masurenkov, 1980). The 3.2 × 4 km caldera is located at an elevation of 615 m above sea level. Eruption events within the AN caldera happened in 6500 BP and 4700 BP, and the most recent event occurred in 1996 (Braitseva, 1998; Belousov and Belousova, 2001). The 1996 eruption started several hours after the onset of the Karymsky eruption. The simultaneous eruption of two vents separated by approximately 6 km was preceded by a M_W 7.1 earthquake that occurred at a distance of about 9–17 km southwest from the volcanoes, immediately prior to the onset of the eruption at Karymsky (Zobin and Levina, 1998). Explosive activity in AN caldera

* Corresponding author.
E-mail address: zhonglu@smu.edu (Z. Lu).

https://doi.org/10.1016/j.jvolgeores.2018.01.011
0377-0273/

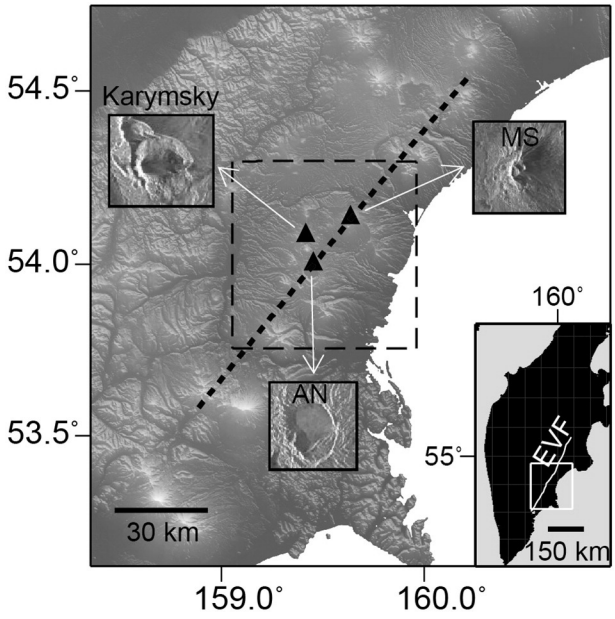

Fig. 1. Shaded relief map of Karymsky Volcanic Center (KVC) area and its vicinity. Black triangle denotes the location of Karymsky Volcano, Akademia Nauk Volcano (AN), and Maly Semyachik Volcano (MS) with insets showing zoomed-in SAR images of each individual center. The dashed box marks the area covered by interferograms shown in Fig. 3. The heavy short dashed line represents the fault. Lower right inset shows location of KVC at the middle of Eastern Volcanic Front (EVF), Kamchatka. The white lines schematically show EVF volcanic belts.

stopped after about 12–14 h of activity (Maguskin et al., 1998; Fazlullin et al., 2000).

Maly Semyachik is a complex stratovolcano located 16 km northeast of Karymsky (Fig. 1). The volcano consists of three coalesced edifices constructed sequentially since ca. 20,000 years BP (Selyangin and Braitseva, 1991). The volcano is situated in the middle of two nested calderas, whose ages are estimated as 1.1 Ma and 20,000 BP (Selyangin and Braitseva, 1991; Bindeman et al., 2010). Historical eruptions partially destroyed the summit of the volcano forming an ~800-meter-diameter crater. At present, the crater is occupied by a turquoise-colored lake, with an elevated temperature and highly acidic composition suggestive of vigorous hydrothermal activity at the bottom, which may be attributed to the presence of a shallow magma system (Selyangin and Braitseva, 1991).

Deformation at KVC has been studied systematically using both triangulation networks and leveling measurements implemented during 1972–2005 (Maguskin et al., 2008 and references therein). The geodetic measurements indicate that the Karymsky and AN areas were experiencing extension during 1972–2005 (Maguskin et al., 2008). Analysis of leveling data acquired during 1972–2005 suggested a deflation with a velocity of 5–9 mm/year during 1996–2001 and inferred a deformation center situated between Karymsky and AN (Maguskin et al., 2008 and references therein).

InSAR has now become a well-established method to investigate volcanic deformation and understand magma supply dynamics at many of the world's volcanoes (e.g., Amelung et al., 2000; Calais et al., 2008; Biggs et al., 2014; Massonnet et al., 1995; Lu et al., 2000, 2005, 2010; Lu, 2007; Lu and Dzurisin, 2014; Pritchard and Simons, 2004; Xu et al., 2015; Yun et al., 2006; Wright et al., 2006). At Kamchatkan volcanoes, InSAR has been used to study ground deformation associated with magmatic intrusion. Lundgren and Lu (2006) successfully observed an episodic magma intrusion event during 2000–2003 at Uzon caldera using Envisat and Radarsat-1 images. Ji et al. (2013) observed a pre-eruption deformation at Kizimen volcano which was caused by a dike intrusion during 2008–2010, about 2 years before the eruption began. Lundgren et al. (2015) observed the dike-intrusion process of the 2012–2013 eruption event at the Tolbachik volcano by InSAR data. No significant deformation was observed using InSAR at several Kamchatkan volcanoes that erupt frequently, like Sheveluch (Pritchard and Simons, 2004; Lundgren and Lu, 2006).

This manuscript presents new InSAR observations of eruptive and non-eruptive deformation at KVC. Two Mogi point pressure sources provide a good fit to the observed deformation. One source is located beneath the area between Karymsky and AN with a depth of 7.0 km, and the other one is situated beneath MS with a depth of 5.8 km. The two magma sources appear to be connected at times, yet show the four stages of activity, i.e. (1) from 2000 to 2004, the Karymsky-AN area deflated and the MS area inflated, (2) from 2004 to 2006, the Karymsky-AN area deflated with ongoing eruption, while the MS area subsided without eruption, (3) from 2006 to 2008, as with 2000–2004, the Karymsky-AN area deflated and the MS area inflated, (4) from 2008 to 2010, the Karymsky-AN area inflated up to 3 cm, and the MS area subsided. These two shallow magma reservoirs may be connected and supplied by a common deep magma source.

2. InSAR data and analysis

Processed radar data were acquired by the Radarsat-1, Envisat, and ALOS satellites, operating at three different wavelengths of 56.6 mm, 56.3 mm, and 236.2 mm, respectively. Taken as a whole, these images constitute 7 different imaging geometries (Table 1). To achieve the best coherent interferograms for KVC, we only chose SAR images acquired during the summer and early fall (from mid-June to mid-October) to avoid coherence loss due to snow and ice. The two-pass InSAR approach (e.g. Massonnet and Feigl, 1998; Rosen et al., 2000) was utilized to form 36 deformation interferograms with reasonably good coherence (Fig. 2). The effects of topography were removed from the interferograms using a filled 3-arc-sec (~90 m) resolution Shuttle Radar Topography Mission (SRTM) digital elevation model (DEM) (Farr and Kobrick, 2000) obtained from the Consultative Group on Inter-national Agricultural Research Consortium for Spatial Information (CGIAR-CSI, http://srtm.csi.cgiar.org). To remove residual orbit errors, a fine estimation of the interferogram baseline was obtained by nonlinear least-square adjustment of the observed phase over presumably stable areas (Rosen et al., 1996; Lu, 2007). For interferograms that are obviously contaminated by topography-correlated atmospheric delays, a linear correction based on topographic height was applied based on phase observations of areas distant from the volcano. Considering low coherence, interferograms were filtered twice using an adaptive filter function based on the local fringe spectrum (Goldstein and Werner, 1998), with the dimensions of the windows at 128×128 and 32×32 pixels, respectively. This filtering strategy removes the high frequency noise efficiently (Nof et al., 2012), and makes the phase unwrapping much considerably easier.

Fig. 3 shows eight examples of interferograms that span time intervals of one year to three years. Together these interferograms map patterns of deformation from 2000 to 2010, and lead to the following observations:

1. The interferograms show little deformation (less than a full color fringe) near Karymsky and AN area during those periods spanning 2000–2003 (Fig. 3a), 2003–2004 (Fig. 3b), 2006–2007 (Fig. 3f), and 2007–2008 (Fig. 3g). In addition, interferograms indicate large

Table 1
Line-of-Sight (LOS) vectors for the 7 different imaging geometries.

Satellite/Track ID	LOS Vector [East, North, Up]
Radarsat1/Beam4	[0.693 −0.107 0.713]
Radarsat1/Beam6	[0.727 −0.103 0.679]
Radarsat1/Beam7	[0.592 −0.111 0.798]
ENVISAT/395	[−0.408 −0.099 0.908]
ENVISAT/059	[0.377 −0.091 0.922]
ALOS/360	[−0.616 −0.111 0.779]
ALOS/030	[0.616 −0.111 −0.779]

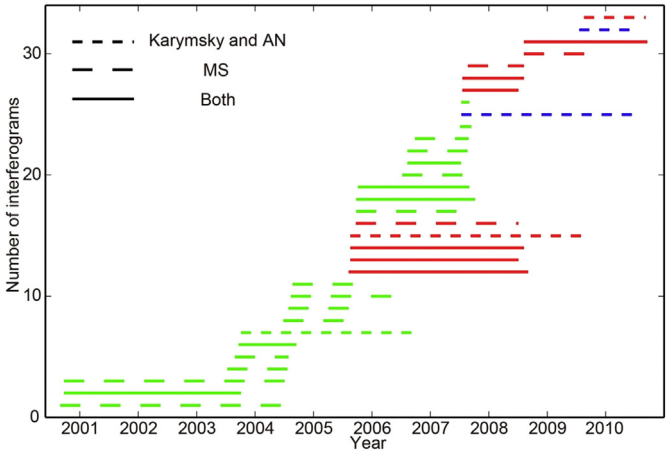

Fig. 2. Temporal intervals of the 33 selected InSAR image pairs which are indicated by length of the lines. The green, red, and blue colors indicate satellite source of images acquired by RadarSat-1, ENVISAT, and ALOS, respectively. Dotted lines with shorter spacing represent the corresponding interferograms which were used to model the magma source beneath Karymsky and AN only (7 total). Dotted lines with longer spacing represent the corresponding interferograms which were used to model the magma source beneath MS only (15 total). Solid lines represent the corresponding interferograms which were used to model two magma sources beneath Karymsky and AN, and MS, respectively (11 total).

deformation (more than a full color fringe) near Karymsky and AN area during 2005–2008 (Fig. 3d, e), with maximum line-of-sight (LOS) enlarging of about 3 cm, while maximum LOS shortening of about 3 cm happened during 2009–2010 (Fig. 3h, i). These fringes are thought to be deformation signals. First, they are unlikely to be atmospheric artifacts, because these interferograms were produced from independent SAR images acquired on different sensors/tracks/dates. Second, the presence of the signals cannot be attributed to DEM errors because the interferograms are constructed with a range of perpendicular baseline lengths.

2. Interferograms from different sensors and tracks show conspicuous deformation signals around MS volcano area (Fig. 3a–g) during 2000–2008, but no similar patterns after 2009 (Fig. 3h, i). Fringes shown in Fig. 3a–b, 3d–g indicate inflation signals around MS volcano with maximum LOS shortening about 6 cm in an area about 15 km in diameter during the periods 2000–2004 and 2006–2008, while Fig. 3c shows a subsidence signal during 2004–2005.
3. The observed deformation around Karymsky, AN, and MS volcano areas did not occur progressively from 2000 to 2010. For example, the Karymsky and AN area subsided during 2000–2008, but inflated during 2009–2010.

3. Deformation modeling and analysis

On the basis of the shapes and radial patterns of the displacement fields, we theorize that the deformation was caused by volume changes in two spherical magma reservoirs, one situated beneath the area between Karymsky and AN, and a second beneath MS. We modeled the displacement fields using a point source of dilation or contraction in an elastic half-space (Mogi, 1958) that includes a correction to account for topographic variation (Williams and Wadge, 1998). In the model, linear terms are introduced to account for any possible phase ramp due to orbital errors (Massonnet and Feigl, 1998). We used the downhill simplex method and Monte Carlo simulations (Press et al., 1992) to estimate optimal parameters and their uncertainties, and the root mean square errors (RMSE) between the observed and modeled interferograms as the prediction-fit criterion.

To determine the two sources of the observed displacements, we employed the following modeling strategy. First, we modeled interferograms to determine the horizontal positions of the deformation sources related to magma injection or extrusion. Fig. 3i (20090817–20100906, ENVISAT Track 395) was chosen to estimate the Mogi source parameters beneath the area between Karymsky and AN because of its best coherence and least apparent atmospheric contaminations, and also because it shows no obvious deformation around the MS volcano. Fig. 4 shows observed (a), modeled (b), and residual (c) interferograms for this Mogi model. The residual interferogram in Fig. 4c is observed (Fig. 4a) minus modeled (Fig. 4b). The modeled interferogram fits the observed interferogram reasonably well. The cross shown in Fig. 4b represents the location of the Mogi source, situated between Karymsky and AN. The horizontal position is well constrained according to the uncertainties shown in Table 2.

Next, Fig. 3e (20050923–20080704, ENVISAT descending track 059) was chosen to study the Mogi source parameters beneath the MS volcano. We masked the MS volcano from Fig. 3e and then modeled the Karymsky and AN area by fixing the horizontal position of the deformation source from Fig. 4b. Fig. 4 shows observed (d), modeled (e), and residual (f) interferograms. The residual interferogram (Fig. 4f) is obtained by removing the modeled (Fig. 4e) one from the observed one (Fig. 4d). The residual interferogram in Fig. 4f was then used to generate the modeled interferogram in Fig. 4g, with a Mogi source beneath southwest of MS volcano. The horizontal coordinates of the deformation sources are shown in Table 2. One thing to be noted is that we only selected two interferograms for modeling the horizontal positions of the two sources. We acknowledge that modeling only two, rather than all the interferograms, may be selective, but this provides a first-order approach to reducing errors in the modeling by only using the best data for each source. Moreover, it is unlikely that the volcanic deformation source moves laterally during a decade-long period (e.g. Lu et al., 2003, 2005).

Finally, we fixed the horizontal position of the deformation sources from Mogi modeling (Fig. 4b and g), and estimated the source depths and volume changes beneath each of the two areas. The area beneath Karmsky and AN was based on 18 interferograms and the area beneath MS was based on 26 interferograms (Fig. 2). The results are shown in Fig. 5a (Karymsky-AN) and 5b (MS). The error bars and circles represent the uncertainty for depth and volume change calculations at one standard deviation, respectively. The estimated average depth of the source beneath the Karymsky-AN area is 7.0 km below sea level (dashed line, Fig. 5a) and for the source beneath MS, it is 5.8 km (Fig. 5b). The depth of the source beneath Karymsky and AN for all the 18 interferograms slightly fluctuated through 2000 to 2010, but the difference was not significant at the 95% confidence level. The depth of the source beneath MS volcano also did not change appreciably based on the 26 interferograms. Taken in total, the two sources remained essentially stationary during the 10-year period of study.

Ambiguity between the two parameters, i.e. depth and volume change, in Mogi model is inherent in inversions of a single component of three dimensional deformation data (Dieterich and Decker, 1975). To address this limitation, we recalculated the volume change parameter for both sources, using the horizontal positions from Fig. 4b and g and the depth values from Fig. 5. Then, we calculated the cumulative source volumes as a function of time. To reduce the number of time steps, SAR images that were acquired within two months of each other were assigned the same acquisition time. For example, images acquired on August 8, 2005 and August 19, 2005 were both assigned an August 2005 acquisition time. This resulted in 9 and 10 image acquisition times for sources beneath Karymsky and AN, and MS volcano, respectively. If we define $\mathbf{V} = (V_1, V_2, \ldots, V_i, \ldots, V_n)$, where V_i is the source volume at the ith acquisition time, then the volume changes indicated by all the interferograms, $\mathbf{L} = (L_1, L_2, \ldots, L_i, \ldots L_m)$, is related to $\mathbf{V}$ by $\mathbf{AV^T} = \mathbf{L^T}$, where $\mathbf{A}$ is a m by n binary matrix. For the source beneath Karymsky and AN, m and n equal 18 and 9, respectively, while for the source beneath MS volcano, m and n are corresponding to 26 and 10, respectively. Unity and null elements in each row correspond to the

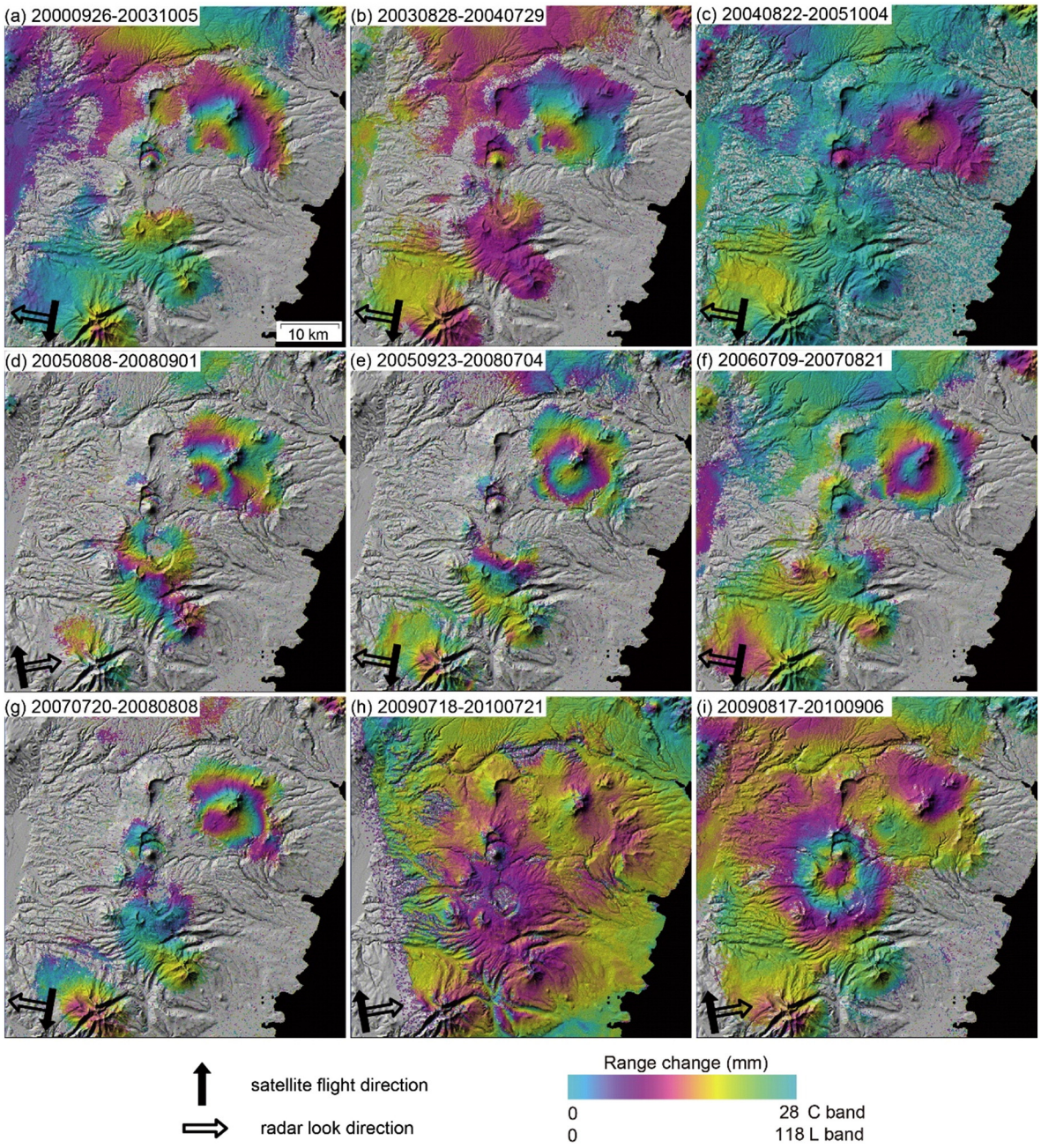

Fig. 3. Representative deformation interferograms of Karymsky Volcanic Center spanning the following periods (date format is yyyymmdd): (a) 20000926–20031005 (Radarsat-1 Beam4), (b) 20030828–20040729 (Radarsat-1 Beam7), (c) 20040822–20051004 (Radarsat-1 Beam7), (d) 20050808–20080901 (ENVISAT Track 395), (e) 20050923–20080704 (ENVISAT Track 059), (f) 20060709–20070821 (Radarsat-1 Beam4), (g) 20070720–20080808 (ENVISAT Track 059), (h) 20090718–20100721 (ALOS PALSAR Path 360), (i) 20090817–20100906 (ENVISAT Track 395). Satellite flight direction and radar look direction are shown by solid and open arrows, correspondingly. Each fringe (full color cycle) represents 28 mm or 118 mm of range change between the ground and satellite for Radarsar-1/ENVISAT (a–f, h) and ALOS (g), respectively. Areas that lack interferometric coherence are uncolored.

temporal coverage for an interferogram. For instance, if the *i*th interferogram spans the period between the second and the third acquisition times, the second and the third columns of the *i*th row should be -1 and 1 corresponding to the duration of the interferogram coverage. We took the source volume corresponding to the first acquisition time (i.e. September 2000) as a reference. A weighting matrix, **w**, was assembled by using the source volume uncertainties for the diagonal elements. This assumes that source volumes estimated from all the interferograms are uncorrelated. The weighted least squares solution (e.g., Lu et al., 2005) for **V** is:

$$\mathbf{V} = \left(\mathbf{A}^{\mathbf{T}}\mathbf{P}\mathbf{A}\right)^{-1}\mathbf{A}^{\mathbf{T}}\mathbf{P}\mathbf{L}^{\mathbf{T}} \quad (1)$$

Using Eq. (1), we estimated the source volumes as a function of time (Fig. 6). It appears that from September 2000 to August 2009 the volume of the source beneath Karymsky and AN (blue bars on Fig. 6) decreased almost linearly with time, although the poor temporal resolution of InSAR images in this area imposes considerable uncertainty to that inference. Since August 2009, the volume of the source beneath Karymsky and AN increased sharply and reached 2.3×10^7 m^3 by August 2010. Our method is similar to those proposed by Biggs et al. (2010), Grandin et al. (2010) and González et al. (2013). To achieve the time-series displacements, Biggs et al. (2010) connected all the interferograms in terms of deformation velocity and solved for incremental displacements. Based on an extensive InSAR data set, Grandin et al. (2010) inverted the locations and shapes of 13 dikes that were active

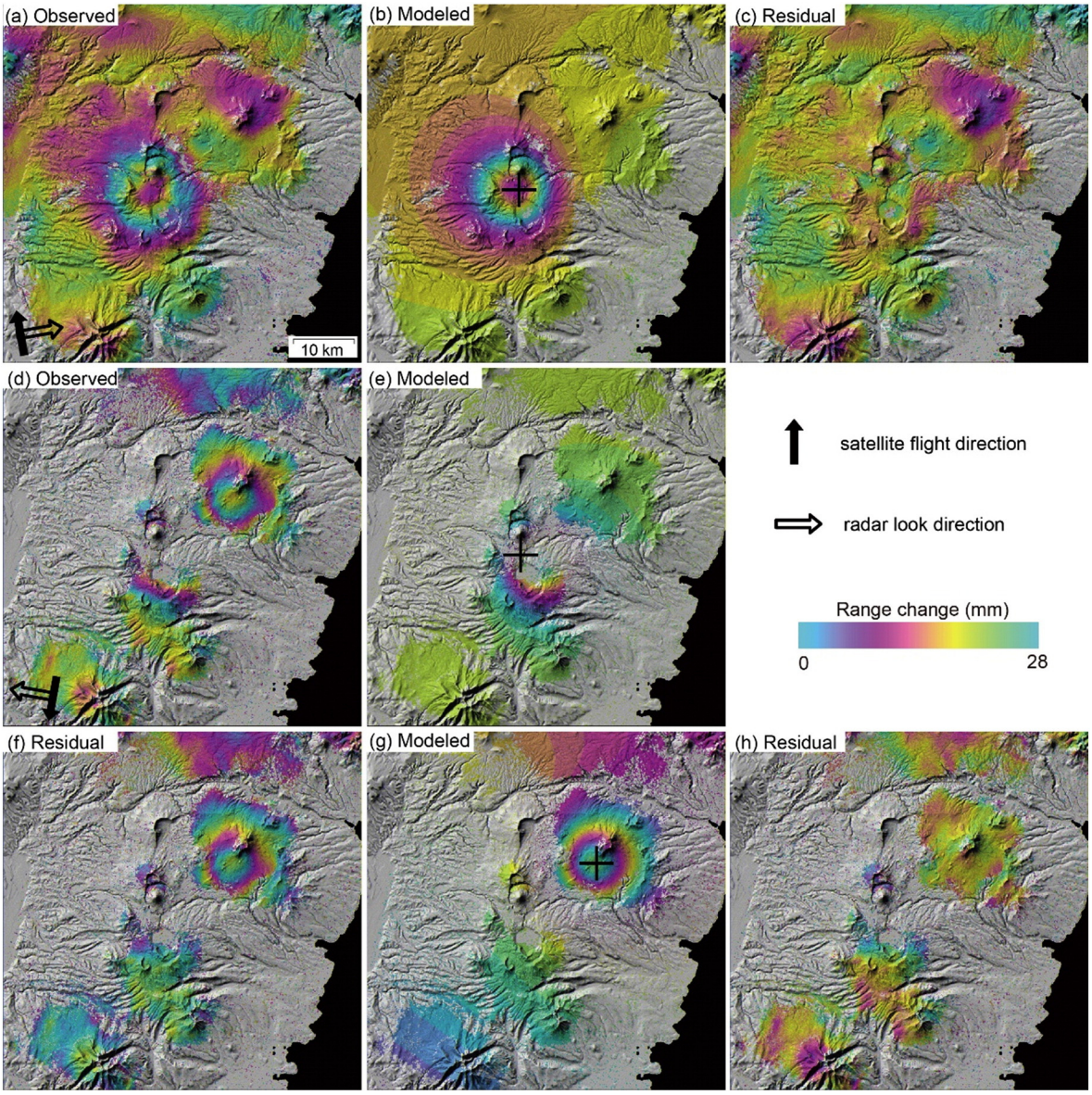

Fig. 4. (a) Observed interferogram for the period spanning 20090817–20100906 (ENVISAT Track 395); (b) synthetic interferogram from Mogi source (indicated by black cross) beneath an area between Akademia Nauk (AN) and Karymsky volcanos that best fits the observed interferogram (a); (c) residual interferogram, which is the difference between observed interferogram (a) and modeled interferogram (b); (d) observed interferogram for the period spanning 20050923–20080704 (ENVISAT Track 059); (e) synthetic interferogram by the Mogi source (indicated by black cross) with horizontal position fixed according to (b); (f) residual interferogram by removing synthetic interferogram (e) from observed interferogram (d); (g) synthetic interferogram from Mogi source (indicated by black cross) beneath MS volcano that best fits the residual interferogram (f); (h) residual interferogram, which is the difference between (f) and (g). Satellite flight direction and radar look direction are shown by solid and open arrows, correspondingly. Each fringe (full color cycle) represents 28 mm of range change between the ground and the satellite or residual. Areas that lack interferometric coherence are uncolored.

during 13 episodes. González et al. (2013) recovered the displacement time series from multi-temporal multi-sensor interferogram observations by minimizing the rate of the source volume changes through a truncated singular value decomposition (TSVD) approach.

The MS volcano did not erupt during the 10-year period of study. However, its magma source volume showed conspicuous fluctuation with time. The magma accumulation rate (red bars on Fig. 6) decreased from 2.4×10^6 m^3/year during 2000–2004, to -2.2×10^6 m^3/year during 2004–2006. The rate increased again during 2006–2008 to 5.5×10^6 m^3/year, which is more than twice higher than for the period of 2000–2004. Then the magma accumulation rate decreased again to -3.7×10^6 m^3/year during 2008–2010, which is higher than for the 2004–2006 period (Fig. 6).

Table 2
Parameters for the best-fitting Mogi sources. Uncertainties show 95% confidence.

Parameters	Karymsky-Akademia Nauk (AN)	Maly Semyachik (MS)
X coordinate (km)	25.99 ± 0.06	36.98 ± 0.04
Y coordinate (km)	29.02 ± 0.08	38.45 ± 0.08
Depth (km)	6.3 ± 0.2	7.0 ± 0.6
Volume (1×10^6 m^3)	8.77 ± 0.3	14.31 ± 0.8

Note: The reference for the horizontal coordinates (X, Y) is the southwestern corner of the area shown in Fig. 3.

4. Ground based observations

4.1. Local seismicity records

The only permanent seismic station in the area is located at the southern flank of the Karymsky Volcano at a distance of 1.5 km from the eruptive vent and is capable of detecting seismic events caused by individual volcanic explosions (Fig. 7a). All other seismic stations are

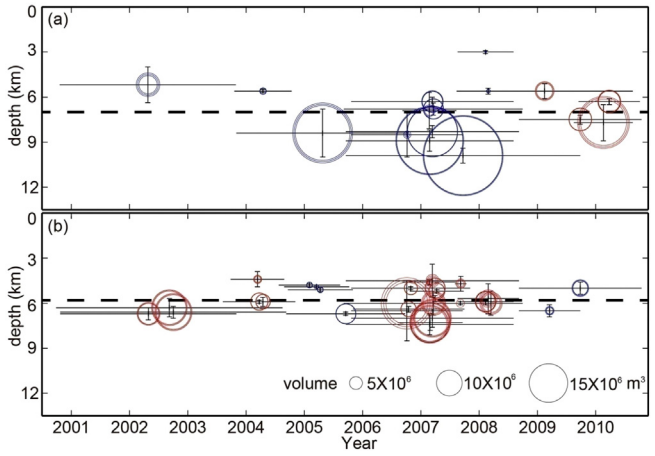

Fig. 5. Estimated volume changes and depths of magma reservoirs beneath Karymsky and AN (a), and MS volcano (b) using the horizontal positions of modeled sources from Fig. 4b and g. Error bars and circles represent one standard deviation uncertainties for depth and volume change of source, respectively. Blue and red circles represent deflation and inflation interferograms, respectively. Horizontal bars denote the time span for each interferogram. The average depths (dotted lines) are 7.0 km and 5.8 km for Karymsky and AN, and MS volcano, respectively.

located at the distance of more than 100 km from KVC. As a consequence, the locations and depths of earthquake epicenters can be determined reliably only for earthquakes of magnitude 2.5 and higher (e.g. Chebrov et al., 2013). Earthquake locations recorded from January 2000 to January 2011 in the KVC area are shown in Fig. 7a and b. The epicenters appear to be concentrated along the North-East trending plane, which orientation generally coincides with the orientation of the Eastern Volcanic Front of Kamchatka. There are two apparent aseismic zones starting at 6–7 km depth beneath Karymsky and MS volcanoes (Fig. 7b), which is comparable to our InSAR-derived magma source depth (Fig. 5). The number of earthquakes recorded by KRY seismic station was elevated during the 2002–2008 period (Fig. 8), thus suggesting that this time period was characterized by elevated explosive activity at Karymsky Volcano.

4.2. GPS measurements

Geodetic surveys at the Karymsky and AN areas have been conducted systematically, every year from 1972 to 1996 (Maguskin et al., 1998). Since 1996 the same sites have been surveyed by GPS campaigns (Bahtiyarov and Maguskin, 2008). During the 2000–2007 period twelve GPS sites have been measured twice a year. The KR9 site located at the Karymsky Volcano Station has been chosen as a benchmark site and has been measured continuously during each GPS campaign. The relative movement of the KR9 site during the period from 2000 to 2007 is shown on Fig. 8. The site moved continuously to the SSW direction, which is consistent with the regional tectonics. The vertical displacement of the site is local and related to volcanic deformations (Bahtiyarov and Maguskin, 2008). Most interestingly, from 2004 to 2008 the KR9 site experienced continuous gradual subsidence, which is consistent with our InSAR results. However, the GPS and InSAR trends are different between 2000 and 2004. Two possible reasons may account for the discrepancy. Two possible reasons may account for the discrepancy. First, GPS and InSAR observations were not taken at the same time, therefore, other errors, for example, seasonal variations may be introduced to the results. Second, the GPS station, located at a place where the InSAR coherence is poor, can record localized deformation such as landslide movement.

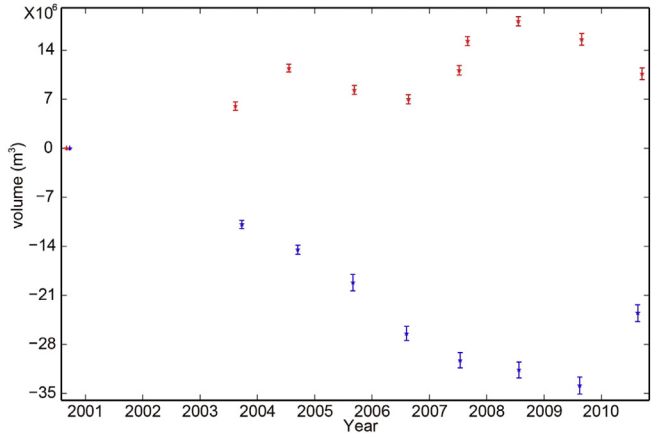

Fig. 6. Estimated magma volumes as a function of time from 2000 to 2010. The volume changes of the magma reservoirs beneath the Karymsky-AN and MS volcano are shown in blue and red colors, respectively. Error bars represent one standard deviation for volume estimates.

4.3. Petrological analyses

Petrological and geochemical studies of the erupted products provide independent information about magma storage areas and magma plumbing processes (e.g. Jay et al., 2014). For us, petrological study of the eruptive products of Karymsky and AN indicated that the current period of eruptive activity at Karymsky started in 1996 with a basaltic recharge, which introduced into the andesitic magma reservoir phenocrysts of calcic plagioclase (Eichelberger and Izbekov, 2000; Izbekov et al., 2004). These calcic plagioclases have been found in Karymsky magmas erupted during the 1996–1999 period as xenocrystic cores surrounded by rims of sodic plagioclase (Izbekov et al., 2002). Importantly, sodic rims showed oscillatory zoning indicative of the growth in nearly steady-state conditions with little fluctuations of pressure and temperature.

Microprobe analysis of the Karymsky andesites erupted in August 2008 indicates that the outermost sodic rims in plagioclase phenocrysts are characterized by the presence of a single conspicuous dissolution boundary followed by a sharp increase of the Ca content (upper section of Fig. 9). In addition, the 2008 Karymsky magmas contain calcic plagioclases, with texture and composition resembling basaltic plagioclases from the beginning of the current eruptive period (lower section of Fig. 9). The widths of sodic rims around calcic cores and dissolution boundaries vary from 15 to 45 μm.

5. Discussion

5.1. Magma plumbing condition at Karymsky and AN

Depths of the source beneath Karymsky and AN for both inflation and deflation periods are similar (Fig. 5a), so we attribute both processes to the same source, i.e. a magma storage zone in the upper crust. All interferograms spanning from 2000 to 2009 show deflation around Karymsky and AN (Fig. 5a), and the source volume decreased linearly with time at a rate of 3.8×10^6 m^3/year (Blue, Fig. 6). On the other hand, the average outflow rate during the first year, i.e. 1996, was 0.35 m^3/s (Walter, 2007), which indicates the annual velocity of discharge was 10.9×10^6 m^3/year. Moreover, the total volume of the eruptive products including pyroclastic and effusive materials, during 1996–2000 was estimated to be 5.03×10^7 m^3 (Ozerov et al., 2003), which indicates the average annual rate of the eruption was about 10.1×10^6 m^3/year. On this basis, we assumed an average steady eruption rate of 10.5×10^6 m^3/year during the studied period. Please note that the source volume deflation rate was 3.8×10^6 m^3/year, about one third of the average steady eruption rate, i.e. 10.5×10^6 m^3/year. In general, the ratio of the erupted volume and volumetric changes in

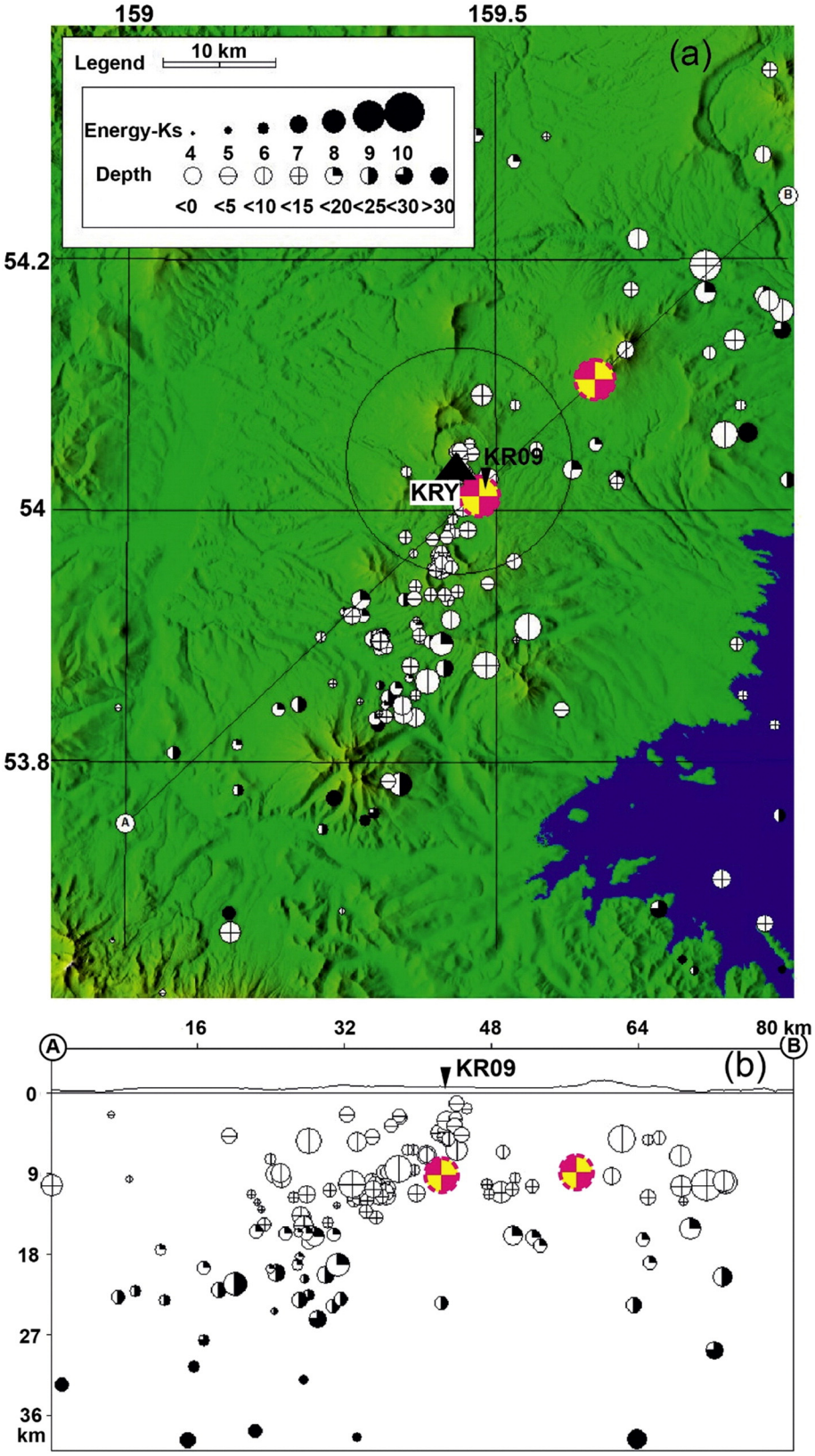

Fig. 7. Area map showing locations/magnitudes (a, top) and depths/magnitudes (b, bottom) of earthquake epicenters recorded from January 2000 to January 2011. Location of the seismic station KRY is shown by black triangle. The large circle with 10 km radius around KRY showing earthquakes which are probably related to Karymsky and AN activities. Location of the GPS campaign site KR9 is indicated by arrow. Red-yellow circles show locations of magma reservoirs based on our InSAR estimates.

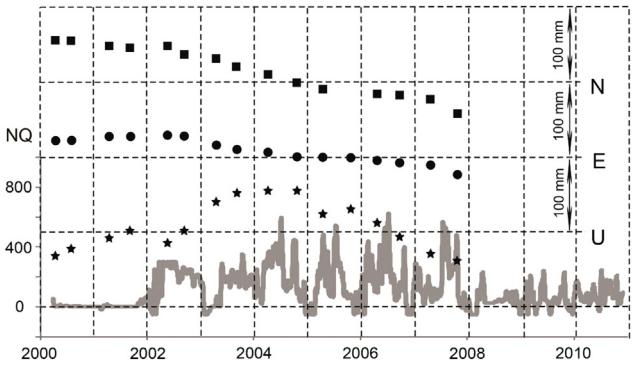

Fig. 8. Gray bold line shows the number of the earthquakes (NQ) recorded by the KRY seismic station. Also shown, with right axis, is relative displacement of the campaign GPS site KR9 during the 2000–2007 period in North (N) (squares), East (E) (circles) and vertical (U) (stars) directions, from Bahtiyarov and Maguskin (2008).

the magma reservoir is about 2 to 5 due to the difference in vesicularity of the erupted and non-erupted material (Sigmundsson et al., 1992). Therefore, the rate of deflation at Karymsky during 2000–2009 period can be explained by continuous magma withdrawal through persistent eruptive activity.

The presence of dissolution boundary in sodic rims of plagioclases, as well as the presence of calcic plagioclases in August 2008 Karymsky magma are consistent with a large input of basaltic material into Karymsky magma reservoir. Although it is difficult to quantify the timing of the recharge, the newly formed sodic rims as thin as 15–45 μm suggests to us that the recharge may have occurred ca. 2–7 months prior to August 2008 considering that the typical plagioclase growth rate at the beginning of the current eruptive period was estimated at 2.5×10^{-9} mm/s (Izbekov et al., 2004). Absence of repeated dissolution boundaries in sodic indicates that there were no substantial basaltic inputs into the shallow magma reservoir of Karymsky-AN between 1996 and 2008, which is consistent with the deflation pattern observed in the InSAR data (Fig. 6).

5.2. Possible mechanisms of deformation at Karymsky Volcanic Center

Usually, the inflation around a volcanic area can be interpreted as the result of magma intrusion or pressurization in the shallow crust (e.g. Lu et al., 2003; Ji et al., 2013). For KVC, we speculate the inflation was associated with magma intrusion. However, volcanic deflation may come from one of many processes, including magma loss due to eruption (e.g. Lu et al., 2000), contraction due to cooling and crystallization of magma body (e.g. Lu et al., 2005), depressurization caused by the release of gas (e.g. Sepe et al., 2007; Fournier, 2008), magma drainage from a shallow reservoir (e.g. Cervelli et al., 2002), or some combination of these. For the Karymsky and AN area, the most likely cause of the deflation is magma withdrawal due to continuous eruptive activities. However, for the MS volcano, which did not erupt during the studied period, the likeliest explanation is contraction due to cooling and crystallization.

Another possible explanation of multiple inflation and deflation events at KVC is draining or lateral transport of magma. The three volcanoes, i.e. Karymsky, AN, and MS, are aligned along the SW–NE trending

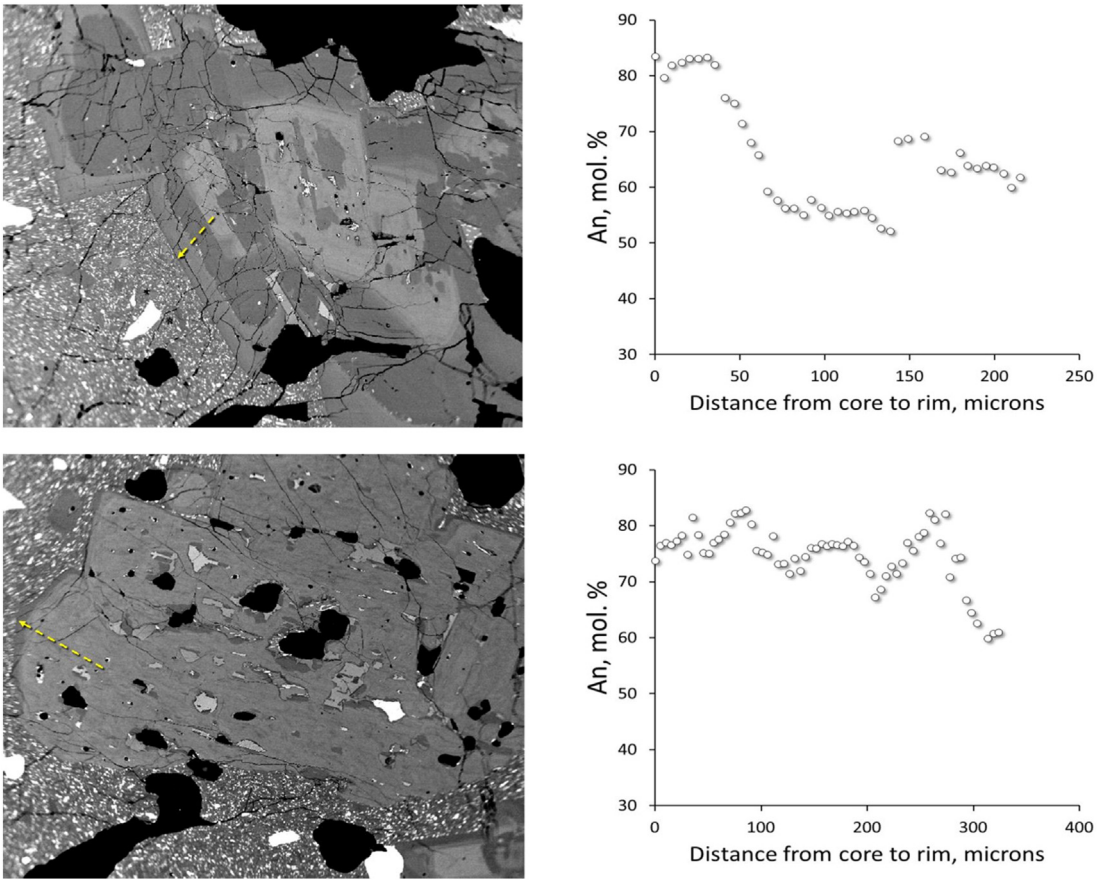

Fig. 9. Back-scattered electron images and corresponding electron microprobe traverses of representative plagioclase phenocrysts from the August 2008 eruptive products of Karymsky volcano: (Upper) plagioclase with patchy calcic core and sodic rim (please note that the rim is characterized by a dissolution boundary and associated jump in An content) and (Lower) calcic plagioclase with coarsely sieved core and ca. 15-μm-wide outermost sodic rim. The yellow dashed lines shown in the electron images indicate the locations of the electron microprobe traverses. Please refer to Izbekov et al. (2002) for the description of analytical procedure.

fracture zone, which is thought to channel the magma to the surface (Zobin and Levina, 1998; Zobin et al., 2003; Walter, 2007) (Fig. 1). Thus, the two magma chambers beneath Karymsky and AN, and MS may be connected with each other through the fracture zone. On the other hand, seismic, geodetic, and petrological data indicate the presence of two magma chambers beneath Karymsky. The small and shallow magma reservoir is located at a depth of 4–5 km (Gordeev et al., 1998a, 1998b; Izbekov et al., 2004), which may be corresponding to our modeled source beneath the Karymsky and AN, and the large and deep one is located at a depth of 18 km (Maguskin and Sharoglazova, 1993; Maguskin et al., 2008; Fedotov, 1998; Zobin et al., 2003; Walter, 2007). The elevated temperature and acidic composition of the crater lake of the MS volcano indicates the presence of a shallow magma chamber underneath (Zobin and Levina, 1998). Therefore, it is possible that all three volcanoes may share a large, deep magma reservoir, which connects and supplies the two shallow chambers beneath Karymsky and AN, and MS, respectively (Fig. 10). During the 10-year studied period, the two shallow chambers should always fed by the large and deep magma chamber. Local earthquakes with magnitude greater than 2.5 recorded depths primarily between 5 km and 20 km (Fig. 7b), which may indicate that the earthquakes were caused by local stress changes due to magma feeding from the deep reservoir to shallower ones. Specifically, during 2000–2004 and 2006–2008, the Karymsky volcano area deflated because the supply rate of the deep magma chamber was too low to inject enough magma into the Karymsky chamber because of eruptive activities (Fig. 11a). The MS area showed an inflationary deformation because of continuing magma supply and no eruption (Fig. 11a). However, during 2004–2006, the MS area subsided without eruption, while the Karymsky and AN area deflated with ongoing eruption. So we speculate the source beneath Karymsky and AN was fed by the deeper chamber and laterally migrating magma from the source beneath the MS volcano through the fracture zone (Fig. 11b). Similarly, during 2008–2010, the MS area subsided again, but the Karymsky and AN area inflated abruptly, from which we infer the supplying rate from the large deep chamber to the source beneath Karymsky and AN was faster than that before 2008. Meanwhile, magma laterally migrating from the source beneath MS volcano to the source beneath Karymsky and AN also occurred (Fig. 11c). The feeding of an eruption from other reservoirs is not so rare. For example, magma migrating occurred prior to, during, and following the September 1984 eruption event at the Krafla volcano, northeast Iceland. And the shallow chamber beneath the Krafla volcano was fed by three additional magma chambers (Tryggvason, 1986). At El Hierro (Canary Islands), lateral magma migration occurred at a depth of 12–15 km in 2011–2012, which was clearly affected by pre-existing structures that controlled its journey inside the volcanic edifice (Martí et al., 2017).

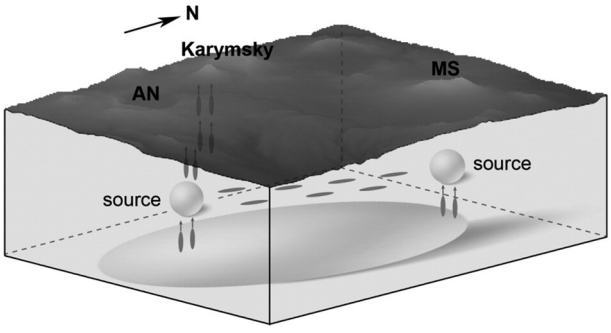

Fig. 10. Cartoon showing magmatic system beneath Karymsky Volcanic Center (not to scale). The two sources are located beneath the center of Karymsky volcano and AN, and the MS volcano, with a depth of 7.0 km and 5.8 km, respectively. The two sources are connected with a conduit and share a large deep source.

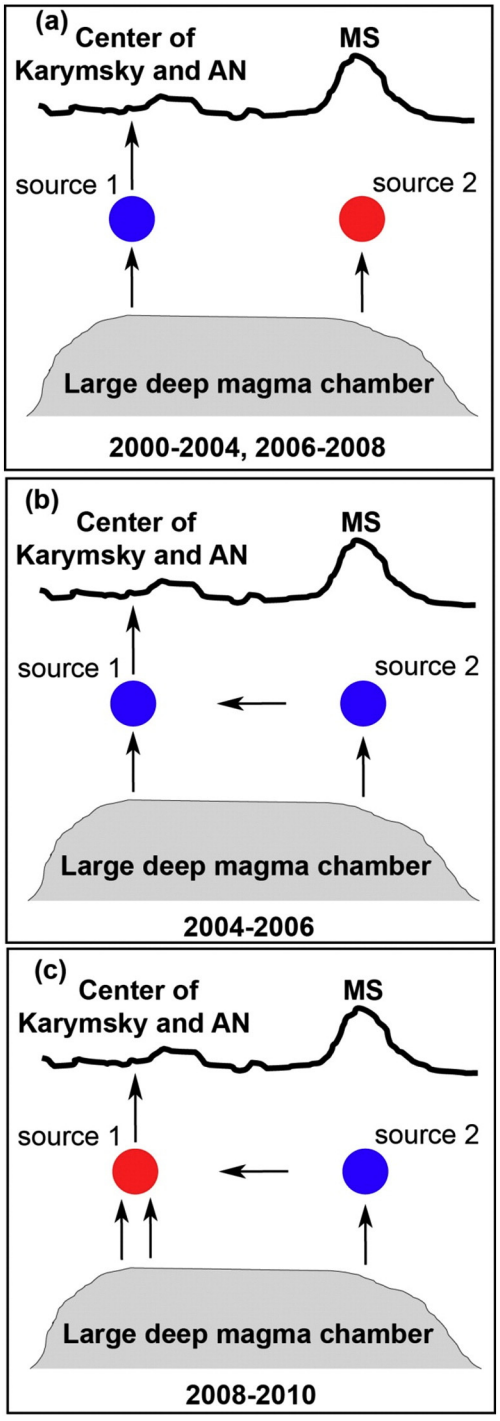

Fig. 11. Schematic sequence of the deformation development around Karymsky Volcanic Center from 2000 to 2010 (not to scale). (a) 2000–2004 and 2006–2008, (b) 2004–2006, (c) 2008–2010. Arrows represent the magma migration paths. Red circles indicate inflation and blue circles indicate deflation.

It is clear that volcano deformation events occur frequently without eruption. For example, Campi Flegrei has been continuously deforming for decades showing uplift and subsidence (Lundgren et al., 2001; Vilardo et al., 2010). Yellowstone caldera underwent an obvious magma migration event during 1992–1997 (Wicks et al., 1998). And, California's Long Valley caldera has been conducting magma unrest with nonlinear deformation characteristics (Hooper et al., 2004; Tizzani et al., 2007, 2009).

6. Conclusions

Multitemporal InSAR images from 3 different radar satellites have been used to map the deformation of KVC during 2000–2010. Two Mogi point pressure sources provide a good fit to the observed deformation. One source is located beneath an area between Karymsky and AN at a depth of 7.0 km, and the second is situated beneath MS at a depth of 5.8 km.

Although simple elastic source models do not account for known complexities of the real Earth, they can provide insights into the behavior of real volcanoes. This study provides details of the activity around the KVC, encompassing the Karymsky, AN, and MS volcano areas, during 2000–2010, as follows:

(1) from 2000 to 2004, the Karymsky-AN area deflated and the MS area inflated,
(2) from 2004 to 2006, the Karymsky-AN area deflated with ongoing eruption, while the MS area subsided without eruption,
(3) from 2006 to 2008, as with 2000–2004, the Karymsky-AN area deflated and the MS area inflated,
(4) from 2008 to 2010, the Karymsky-AN area inflated up to 3 cm, and the MS area subsided.

The InSAR-derived deformation fields can illuminate the shallow magmatic system beneath the KVC. The two magma sources appear to be connected at times, yet show the four stages of activity as mentioned above. The two shallow sources may be supplied by a common huge and deep magma chamber. Also, the two shallow sources are connected to each other through the fracture zone.

No field-based measurements of surface displacement have been made around many Kamchatka volcanoes due to their persistently inclement weather, and displacements inferred from SAR data are therefore all we can currently use to constrain the movement of subsurface magma or hydrothermal fluids. Another advantage of InSAR is its ability to look back at older stored data, which extends the monitoring time scale for Kamchatka volcanoes.

Acknowledgements

The first author would like to thank the China Scholarship Council for funding a one-year InSAR study at the Cascades Volcano Observatory, U.S. Geological Survey (USGS) (2011419028). Lingyun Ji was supported by the National Natural Science Foundation of China (41604015) and the Spark Programs of Earthquake Science from China Earthquake Administration (XY17059); Zhong Lu is supported by the Shuler-Foscue Endowment at Southern Methodist University. ENVISAT SAR data are copyrighted by ESA and were provided by ESA under CAT1-2765. Radarsat-1 SAR data are copyrighted by the Canadian Space Agency (CSA) and were provided by the Alaska Satellite Facility (ASF). ALOS SAR data are copyrighted by JAXA/METI and were provided by ASF and JAXA. Comments from Editor-in-Chief Jurgen Neuberg, Paul Lundgren and an anonymous reviewer improved the manuscript.

References

Amelung, F., Jonsson, S., Zebker, H., Segall, P., 2000. Widespread uplift and 'trapdoor' faulting on Galapagos volcanoes observed with radar interferometry. Nature 407 (6807), 993–996.

Bahtiyarov, V.F., Maguskin, M.A., 2008. GPS monitoring of Karymsky Volcano. Proceedings of the Volcanologist Day Conference, March 30, 2008. Institute of Volcanology and Seismology, Petropavlovsk-Kamchatsky, pp. 28–33 (in Russian).

Belousov, A., Belousova, M., 2001. Eruptive process, effects and deposits of the 1996 and ancient basaltic phreatomagmatic eruptions in Karymskoye lake, Kamchatka, Russia. Special Publication of the International Association of Sedimentologists 30, 35–60.

Biggs, J., Lu, Z., Fournier, T., Freymueller, J.T., 2010. Magma flux at Okmok volcano, Alaska, from a joint inversion of continuous GPS, campaign GPS, and interferometric synthetic aperture radar. J. Geophys. Res. Solid Earth 115 (B12), 424–440.

Biggs, J., Ebmeier, S.K., Aspinall, W.P., Lu, Z., Pritchard, M.E., Sparks, R.S.J., Mather, T.A., 2014. Global link between deformation and volcanic eruption quantified by satellite imagery. Nat. Commun. 5 (4), 3471.

Bindeman, I.N., Leonov, V.L., Izbekov, P.E., Ponomareva, V.V., Watts, K.E., Shipley, N.K., Perepelov, A.B., Bazanova, L.I., Jicha, B.R., Singer, B.S., Schmitt, A.K., Portnyagin, M.V., Chen, C.H., 2010. Large-volume silicic volcanism in Kamchatka: Ar-Ar and U-Pb ages, isotopic, and geochemical characteristics of major pre-Holocene caldera-forming eruptions. J. Volcanol. Geotherm. Res. 189 (1–2), 57–80.

Braitseva, O.A., 1998. Phreatomagmatic eruption in Lake Karymskoe (East Kamchatka) ~6500 ^{14}C years BP and Holocene episodes of basalt magma injection under the Karymsky area. J. Volcanol. Seismol. 19 (5), 685–692.

Braitseva, O.A., Melekestsev, I.V., 1991. Eruptive history of Karymsky Volcano, Kamchatka, USSR, based on tephra stratigraphy and ^{14}C dating. Bull. Volcanol. 53 (3), 195–206.

Calais, E., d'Oreye, N., Albaric, J., Deschamps, A., Delvaux, D., Deverchere, J., Ebinger, C., Ferdinand, R.W., Kervyn, F., Macheyeki, A.S., Oyen, A., Perrot, J., Saria, E., Smets, B., Stamps, D.S., Wauthier, C., 2008. Strain accommodation by slow slip and dyking in a youthful continental rift, East Africa. Nature 456 (7223), 783.

Cervelli, P., Segall, P., Amelung, F., Owen, H., Miklius, S., Lisowski, A., 2002. The 12 September 1999 Upper East Rift Zone dike intrusion at Kilauea Volcano, Hawaii. J. Geophys. Res. Solid Earth 107 (B7) (ECV 3-1–ECV 3-13).

Chebrov, V.N., Droznin, D.V., Kugaenko, Y.A., Levina, V.I., Senyukov, S.L., Sergeev, V.A., Shevchenko, Yu.V., Yashchuk, V.V., 2013. The system of detailed seismological observations in Kamchatka in 2011. J. Volcanol. Seismol. 7 (1), 16–36.

Dieterich, J.H., Decker, R.W., 1975. Finite element modeling of surface deformation associated with volcanism. J. Geophys. Res. 80, 4094–4102.

Eichelberger, J.C., Izbekov, P.E., 2000. Eruption of andesite triggered by dyke injection: contrasting cases at Karymsky volcano. Kamchalka and Mt. Katmai, Alaska. Philos. Trans. R. Soc. Lond. A 358, 1465–1485.

Farr, T.G., Kobrick, M., 2000. Shuttle Radar Topography Mission produces a wealth of data. Eos. Trans. AGU 81 (48), 583–585.

Fazlullin, S.M., Ushakov, S.V., Shuvalov, R.A., Aoki, M., Nikolaeva, A.G., Lupikina, E.G., 2000. The 1996 subaqueous eruption at Academii Nauk volcano (Kamchatka) and its effects on Karymsky lake. J. Volcanol. Geotherm. Res. 91, 181–193.

Fedotov, S.A., 1998. Study and mechanism of the simultaneous 1996 Karymsky Volcano and Akademii Nauk caldera eruptions in Kamchatka. J. Volcanol. Seismol. 19 (5), 525–566.

Firstov, P.P., Fee, D., Makhmudov, E.R., 2013. The explosive activity of Karymskii volcano, Kamchatka: acoustic and seismic observations. J. Volcanol. Seismol. 7 (4), 252–264.

Fischer, T.P., Roggensack, K., Kyle, P.R., 2002. Open and almost shut case for explosive eruptions: vent processes determined by SO2 emission rates at Karymsky volcano, Kamchatka. Geology 30 (12), 1059–1062.

Flower, V.J.B., Kahn, R.A., 2017. Assessing the altitude and dispersion of volcanic plumes using MISR multi-angle imaging from space: sixteen years of volcanic activity in the Kamchatka peninsula, Russia. J. Volcanol. Geotherm. Res. 337, 1–15.

Fournier, T.J., 2008. Analysis and interpretation of volcano deformation in Alaska: studies from Okmok and Mt. Veniamin of Volcanoes. Dissertations & Theses - Gradworks. University of Alaska Fairbanks.

Global Volcanism Program, 2016. Report on Karymsky (Russia). In: Sennert, S.K. (Ed.), Weekly Volcanic Activity Report, 19 October–25 October 2016. Smithsonian Institution and US Geological Survey.

Goldstein, R.M., Werner, C.L., 1998. Radar interferogram filtering for geophysical applications. Geophys. Res. Lett. 25 (21), 4035–4038.

González, P.J., Samsonov, S.V., Susi, P., Tiampo, K.F., Pietro, T., Francesco, C., et al., 2013. Magma storage and migration associated with the 2011–2012 El hierro eruption: implications for crustal magmatic systems at oceanic island volcanoes. J. Geophys. Res. Solid Earth 118 (8), 4361–4377.

Gordeev, E.I., Droznin, D.V., Kasahara, M., Levina, V.I., Leonov, V.L., Miyamachi, H., Okayama, M., Saltykov, V.A., Sinitsyn, V.I., Chebrov, V.N., 1998a. Seismic events associated with the 1996 volcanic eruptions in the Karymsky volcanic center. J. Volcanol. Seismol. 19 (5), 713–735.

Gordeev, E.I., Lees, J.M., Ripepe, M., 1998b. No resonating conduit at Karymsky Volcano. AGU 1998 Fall Meeting, 79. American Geophysical Union, Washington, DC, United States (p. 595. 45, Suppl.).

Grandin, R., Socquet, A., Jacques, E., Mazzoni, N., Chabalier, J.B.D., King, G.C.P., 2010. Sequence of rifting in afar, manda-hararo rift, ethiopia, 2005–2009: time-space evolution and interactions between dikes from interferometric synthetic aperture radar and static stress change modeling. J. Geophys. Res. Solid Earth 115 (B10), 297–326.

Hooper, A., Zebker, H., Segall, P., Kampes, B., 2004. A new method for measuring deformation on volcanoes and other natural terrains using InSAR persistent scatterers. Geophys. Res. Lett. 31 (23), L23611.

Izbekov, P.E., Eichelberger, J.C., Patino, L.C., Vogel, T.A., Ivanov, B.V., 2002. Calcic cores of plagioclase phenocrysts in andesite from Karymsky volcano: evidence for rapid introduction by basaltic replenishment. Geology 30, 799–802.

Izbekov, P.E., Eichelberger, J.C., Ivanov, B.V., 2004. The 1996 eruption of Karymsky Volcano, Kamchatka; historical record of basaltic replenishment of an andesite reservoir. J. Petrol. 45 (11), 2325–2345.

Jay, J., Costa, F., Pritchard, M., Lara, L., Singer, B., Herrin, J., 2014. Locating magma reservoirs using InSAR and petrology before and during the 2011–2012 Cordón Caulle silicic eruption. Earth Planet. Sci. Lett. 395, 254–266.

Ji, L.Y., Lu, Z., Dzurisin, D., Sergey, S., 2013. Pre-eruption deformation caused by dike intrusion beneath Kizimen volcano, Kamchatka, Russia, observed by InSAR. J. Vol. and Geother. Reas. 256, 87–95.

Lopez, T., Fee, D., Prata, F., Dehn, J., 2014. Characterization and interpretation of volcanic activity at Karymsky volcano, Kamchatka, Russia, using observations of infrasound, volcanic emissions, and thermal imagery. Geochem. Geophys. Geosyst. 14 (12), 5106–5127.

Lu, Z., 2007. InSAR imaging of volcanic deformation over cloud-prone areas - Aleutian islands. Photogramm. Eng. Remote. Sens. 73 (3), 245–257.
Lu, Z., Dzurisin, D., 2014. InSAR imaging of Aleutian Volcanoes: monitoring a volcanic arc from space. Springer Praxis Books, Geophysical Sciences, ISBN 978-3-642-00347-9. Springer (390 pp).
Lu, Z., Mann, D., Freymueller, J., Meyer, D., 2000. Synthetic aperture radar interferometry of Okmok volcano, Alaska: radar observations. J. Geophys. Res. 105 (10), 10,791–10,806.
Lu, Z., Masterlark, T., Dzurisin, D., Rykhus, R., Wicks Jr., C., 2003. Magma supply dynamics at Westdahl volcano, Alaska, modeled from satellite radar interferometry. J. Geophys. Res. 108 (B7), 2354.
Lu, Z., Masterlark, T., Dzurisin, D., 2005. Interferometric synthetic aperture radar study of Okmok volcano, Alaska, 1992–2003: magma supply dynamics and postemplacement lava flow deformation. J. Geophys. Res. 110, B02403.
Lu, Z., Dzurisin, D., Biggs, J., Wicks, J.C., McNutt, S., 2010. Ground surface deformation patterns, magma supply, and magma storage at Okmok volcano, Alaska, from InSAR analysis: 1. Intereruption deformation, 1997–2008. J. Geophys. Res. 115, B00B02.
Lundgren, P., Lu, Z., 2006. Inflation model of Uzon caldera, Kamchatka, constrained by satellite radar interferometry observations. Geophys. Res. Lett. 33, L06301.
Lundgren, P., Usai, S., Sansosti, E., Lanari, R., Tesauro, M., Fornaro, G., Berardino, P., 2001. Modeling surface deformation observed with SAR interferometry at Campi Flegrei caldera. J. Geophys. Res. 106, 19355–19367.
Lundgren, P., Kiryukhin, A., Milillo, P., Samsonov, S., 2015. Dike model for the 2012–2013 Tolbachik eruption constrained by satellite radar interferometry observations. J. Volcanol. Geotherm. Res. 307, 79–88.
Maguskin, M.A., Sharoglazova, G.A., 1993. Ground surface deformation in Karymskiy volcanic area. J. Volcanol. Seismol. 14 (4), 450–470.
Maguskin, M.A., Fedotov, S.A., Levin, V.E., Bakhtiarov, V.F., 1998. Ground surface deformation caused by seismic and volcanic activity in the Karymsky volcanic center during January 1996. J. Volcanol. Seismol. 19 (5), 637–654.
Maguskin, M.A., Fedotov, S.A., Levin, V.E., Bakhtiarov, V.F., 2008. Deformations related to a large (M 6.9) earthquake, the magma discharge, and eruptions in the Karymskii volcanic center in 1996–2005. J. Volcanol. Seismol. 2 (5), 322–339.
Martí, J., Villaseñor, A., Geyer, A., López, C., Tryggvason, A., 2017. Stress barriers controlling lateral migration of magma revealed by seismic tomography. Sci. Rep. 7, 40757.
Massonnet, D., Feigl, K., 1998. Radar interferometry and its application to changes in the Earth's surface. Rev. Geophys. 36, 441–500.
Massonnet, D., Briole, P., Arnaud, A., 1995. Deflation of Mount Etna monitored by spaceborne radar interferometry. Nature 375, 567–570.
Masurenkov, Yu.P., 1980. Volcanic centers: formation, dynamics, properties (Karymsky Structure). Nauka, Moscow, USSR (300 pp in Russian).
Mogi, K., 1958. Relations between the eruptions of various volcanoes and the deformations of the ground surface around them. Bull. Earthq. Res. Inst., Univ. Tokyo 36, 99–134.
Muravyev, Y.D., Fedotov, S.A., Budnikov, V.A., Ozerov, A.Y., Maguskin, M.A., Dvigalo, V.N., Andreev, V.Il, Ivanov, V.V., Kartasheva, L.A., Markov, I.A., 1998. Activity in the Karymsky center in 1996: summit eruption at Karymsky and phreatomagmatic eruption in the Akademii Nauk Caldera. J. Volcanol. Seismol. 19 (5), 567–604.
Nof, R.N., Ziv, A., Doin, M.P., Baer, G., Fialko, Y., Wdowinski, S., Eyal, Y., Bock, Y., 2012. Rising of the lowest place on Earth due to Dead Sea water-level drop: evidence from SAR interferometry and GPS. J. Geophys. Res. 117, B05412.
Ozerov, A., Ispolatov, I., Lees, J., 2003. Modeling Strombolian eruptions of Karymsky volcano, Kamchatka, Russia. J. Volcanol. Geotherm. Res. 122, 265–280.
Press, W., Teukolsky, S., Vetterling, W., Flannery, B., 1992. Numerical recipes in C. The Art of Scientific Computing. Cambridge Univ. Press, New York (994).
Pritchard, M.E., Simons, M., 2004. Surveying volcanic arcs with satellite radar interferometry: the central Andes, Kamchatka, and beyond. GSA Today 14 (8), 4–11.
Rosen, P., Hensley, S., Zebker, H., Webb, F.H., Fielding, E.J., 1996. Surface deformation and coherence measurements of Kilauea Volcano, Hawaii, from SIR-C radar interferometry. Journal of Geophysical Rearch 101, 23109–23125.
Rosen, P.A., Hensley, S., Joughin, I.R., Li, F.K., Madsen, S.N., Rodriguez, E., Goldstein, R.M., 2000. Synthetic aperture radar interferometry. Proc. IEEE 88, 333–380.
Rowell, C.R., Fee, D., Szuberla, C.A.L., Arnoult, K., Matoza, R.S., Firstov, P.P., Kim, K., Makhmudov, E., 2014. Three-dimensional volcano-acoustic source localization at Karymsky volcano, Kamchatka, Russia. J. Volcanol. Geotherm. Res. 283 (15), 101–115.
Selyangin, O.B., Braitseva, O.A., 1991. Maly Semiachik Volcano. Active Volcanoes of Kamchatka. Nauka Publishers, Moscow, pp. 162–179.
Sepe, V., Atzori, S., Ventura, G., 2007. Subsidence due to crack closure and depressurization of hydrothermal systems: a case study from Mt Epomeo (Ischia Island, Italy). Terra Nova 19 (2), 127–132.
Sigmundsson, F., Einarsson, P., Bilham, R., 1992. Magma chamber deflation recorded by the Global Positioning System: the Hekla 1991 eruption. Geophys. Res. Lett. 19 (14), 1483–1486.
Tizzani, P., Berardino, P., Casu, F., Euillades, P., Manzo, M., Ricciardi, G.P., Zeni, G., Lanari, R., 2007. Surface deformation of Long Valley caldera and Mono Basin, California, investigated with the SBAS-InSAR approach. Remote Sens. Environ. 108, 277–289.
Tizzani, P., Battaglia, M., Zeni, G., Atzori, S., Berardino, P., Lanari, R., 2009. Uplift and magma intrusion at Long Valley caldera from InSAR and gravity measurements. Geology 37 (1), 63–66.
Tryggvason, E., 1986. Multiple magma reservoirs in a rift zone volcano: ground deformation and magma transport during the September 1984 eruption of Krafla, Iceland. J. Volcanol. Geotherm. Res. 28, 1–2), 1–44.
Vilardo, G., Isaia, R., Ventura, G., De Martino, P., Terranova, C., 2010. InSAR Permanent Scatterer analysis reveals fault re-activation during inflation and deflation episodes at Campi Flegrei caldera. Remote Sens. Environ. 114 (10), 2373–2383.
Walter, T.R., 2007. How a tectonic earthquake may wake up volcanoes: stress transfer during the 1996 earthquake-eruption sequence at the Karymsky Volcanic Group, Kamchatka. Earth Planet. Sci. Lett. 264, 347–359.
Wicks, C., Thatcher, W., Dzurisin, D., 1998. Migration of fluids beneath Yellowstone caldera inferred from satellite radar interferometry. Science 282, 458–462.
Williams, C.A., Wadge, G., 1998. The effects of topography on magma chamber deformation models: application to Mt. Etna and radar interferometry. Geophys. Res. Lett. 25, 1549–1552.
Wright, T.J., Ebinger, C., Biggs, J., Ayele, A., Yirgu, G., Keir, D., Stork, A., 2006. Magma-maintained rift segmentation at continental rupture in the 2005 Afar dyking episode. Nature 442, 291–294.
Xu, W., Ruch, J., Jónsson, S., 2015. Birth of two volcanic islands in the southern Red Sea. Nat. Commun. 6 (12), 7104.
Yun, S., Segall, P., Zebker, H., 2006. Constraints on magma chamber geometry at Sierra Negra Volcano, Galapagos Islands, based on InSAR observations. J. Volcanol. Geotherm. Res. 150 (1–3), 232–243.
Zobin, V.M., Levina, V.I., 1998. Rupture history of the January 1, 1996, Ms 6.6 volcanic earthquake preceding the simultaneous eruption of Karymsky and Akademia Nauk volcanoes in Kamchatka, Russia. J. Geophys. Res. 103 (B8), 18,315–18,324.
Zobin, V.M., Levina, V.I., Maguskin, M.A., 2003. Seismicity and crustal deformation preceding the January 1996 eruptions at Karymsky Volcanic Center, Kamchatka. Bull. Volcanol. 65 (7), 477–485.